

Measurement of Temporal Correlations of the Overhauser Field in a Double Quantum Dot

D. J. Reilly¹, J. M. Taylor², E. A. Laird¹, J. R. Petta³, C. M. Marcus¹, M. P. Hanson⁴ and A. C. Gossard⁴

¹ *Department of Physics, Harvard University, Cambridge, MA 02138, USA*

² *Department of Physics, Massachusetts Institute of Technology, Cambridge, MA 02139, USA*

³ *Department of Physics, Princeton University, Princeton, NJ 08544, USA and*

⁴ *Department of Materials, University of California, Santa Barbara, California 93106, USA*

Correlation functions and power spectral densities of Overhauser field fluctuations, resulting from the hyperfine coupling of a separated pair of electrons to local nuclear ensembles, are measured in a few-electron GaAs double quantum dot over a bandwidth of 40 mHz to 1 kHz. Measured spectra show broadband content, from milliseconds to the tens of seconds. Experimental spectra are found to be in excellent agreement with a simple model based on nuclear spin diffusion.

Electron spins in quantum dots are an attractive candidate for quantum information processing [1, 2]. For devices fabricated in GaAs, electron spin couples via the hyperfine interaction to $N \sim 10^6$ spin-3/2 nuclei, giving rise to a fluctuating effective (Overhauser) field \mathbf{B}_{nuc} with rms amplitude $B_{nuc} \sim 1\text{-}3$ mT [3, 4, 5, 6, 7]. This broadband, time-dependent magnetic field is the dominant source of spin dephasing [8, 9] and low field spin relaxation [10, 11, 12] in these systems. The implementation of schemes [13, 14, 15, 16] to avoid or control spin dephasing will require a detailed knowledge of the mechanisms and critical time-scales governing hyperfine fluctuations.

Fluctuating nuclear fields have been investigated in atomic systems [17] using optical Faraday rotation, superconducting quantum interference devices [18] and force-detected magnetic resonance [19]. In quantum dots, dynamic nuclear polarization (DNP) [20, 21, 22, 23] can drive the nuclear system beyond equilibrium to produce fluctuating currents and feedback effects in connection with Pauli spin-blockade [11, 24, 25, 26].

In this Letter, we report measurements of the temporal correlations and power spectral densities of the nuclear environment in a two-electron GaAs double-quantum-dot system. In contrast to previous work [11, 22, 23], we do not drive the nuclear system using DNP, but rather probe the statistical fluctuations of the unpolarized nuclear bath in thermal equilibrium [27, 28]. Fluctuations of the Overhauser field are detected as fluctuations in the dephasing time of a two-electron spin state, making use of high-bandwidth proximal charge sensing [29]. Fluctuations are found to be broadband over the measurement bandwidth, 40 mHz to 1 kHz, and sensitive to an applied magnetic field in the range $B = 0$ to 20 mT. Experimental results are shown to be consistent with a simple diffusion model of nuclear dynamics, also presented here.

The double quantum dot is formed by Ti/Au top gates on a GaAs/Al_{0.3}Ga_{0.7}As heterostructure with a two-dimensional electron gas (2DEG) with density $2 \times 10^{15} \text{ m}^{-2}$ and mobility $20 \text{ m}^2/\text{Vs}$, 100 nm below the surface (Fig. 1(a), inset). This device is different, but nominally identical to the device used in our previous work [8, 23]. Measurements are made in a dilution re-

frigerator configured for high-frequency excitation and readout [29] with a base electron temperature of ~ 120 mK. The conductance G_{QPC} of a proximal radio frequency quantum point contact (rf-QPC) is sensitive to the charge configuration of the double dot. G_{QPC} controls the quality factor of an rf tank circuit, modulating the reflected power of a 220 MHz carrier. Demodulation yields a voltage V_{rf} , proportional to G_{QPC} , that constitutes the charge-sensing signal [29]. The external magnetic field B , is applied perpendicular to the 2DEG.

A schematic energy diagram is shown in Fig. 1(a), indicating the number of electrons (n, m) in the left and right dot. Interdot tunneling, t_c , and detuning, ϵ , from the (2,0)-(1,1) charge degeneracy are separately controllable using top gates. Real-time fluctuations in the hyperfine field are detected by probing the mixing of singlet and triplet states. A cyclic gate-pulse sequence, first described in Ref [8] and shown in Fig. 1(b), prepares new singlets each iteration by configuring the device deep in (2,0), at point (P), where transitions to the ground state singlet (2,0) S , occur rapidly [10]. Electrons are then separated to position S in (1,1) for a time τ_S where the singlet and one of the triplet states are nearly degenerate, and are rapidly mixed by the difference in instantaneous Overhauser magnetic fields between left and right dots, $\Delta \mathbf{B}_{nuc} = \mathbf{B}_{nuc}^l - \mathbf{B}_{nuc}^r$ [8].

In an applied field, the position of S determines whether the singlet becomes nearly degenerate with the $m_s = 0$ triplet, T_0 , which occurs at large negative detuning (green line in Fig. 1(b)), or with the T_+ triplet, which occurs at a smaller negative field-dependent value of detuning (red line in Fig. 1(b)). Following separation, a projective measurement of the two-spin state is performed by pulsing to position M in (2,0) for time $\tau_M = 5 \mu\text{s}$. Only the S state can make the transition to the (2,0) charge configuration within τ_M ; this charge transition is then detected by the rf-QPC.

Figures 1(c) and 1(d) show the time-averaged sensing signal, V_{rf} , as a function of gate biases V_L and V_R . Once calibrated, V_{rf} gives the probability $1 - P_S$ that a prepared singlet evolved into a triplet during the separation time τ_S . Inside the readout triangle (see Fig. 1(c)), triplet states remain blocked in (1,1) for a time $T_1 \gg \tau_M$

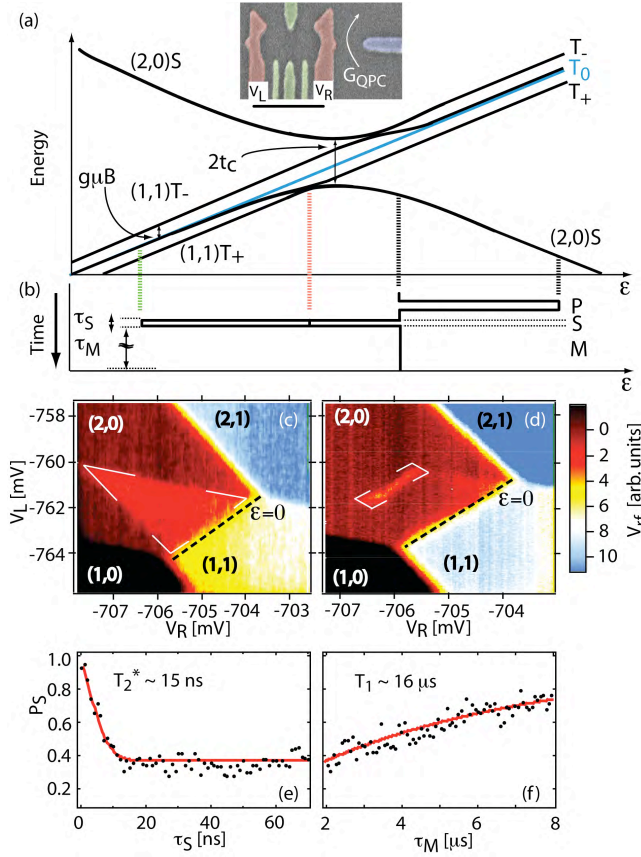


FIG. 1: (Color online) (a) Schematic energy diagram of the two-electron system. Inset: false-color SEM image of a double-dot with integrated rf-QPC charge sensor similar to the one measured (scale bar is 500 nm). (b) Gate-pulse cycle that is used to prepare (P) the (2,0) singlet, separate (S) into (1,1), either to the S - T_0 degeneracy (green dashed line) or the S - T_+ degeneracy (red dashed line), and return to (2,0) for measurement (M). (c) rf-QPC readout, V_{rf} , around the (1,1)-(2,0) transition during application of the cyclic gate-pulse sequence, showing the readout triangle indicated with white lines ($B = 0$ mT, $\tau_S = 50$ ns). A background plane has been subtracted. (d) V_{rf} as in (c), but for S at the S - T_+ degeneracy ($B = 10$ mT). (e) Average value of $P_S(\tau_S)$ at $B = 0$, $\tau_M = 2$ μ s. Red line is a fit to the theoretical gaussian form. (f) Average value of $P_S(\tau_M)$ showing contrast dependence, $\tau_S = 50$ ns. Red line is a fit to the exponential form (see main text).

[10]. Similarly, inside the rectangular region indicated in Fig. 1(d), the prepared singlet mixes with T_+ and becomes blocked in (1,1). Calibration of V_{rf} uses the signal in (2,0) outside the readout triangle, where fast spin-independent relaxation occurs via (1,0) or (2,1), to define $P_S = 1$, and the region within (1,1) to define $P_S = 0$.

Fitting $P_S(\tau_S)$ averaged over tens of seconds with the theoretical gaussian form (Fig. 1(e)) gives $T_2^* = \hbar/(g\mu_B B_{nuc}) \sim 15$ ns corresponding to $B_{nuc} \sim 1.6$ mT ($N \sim 6 \times 10^6$) [8, 30], here g is the electron g -factor and μ_B is the Bohr magneton. The effect of finite T_1 on the calibration of P_S can be accounted by a factor

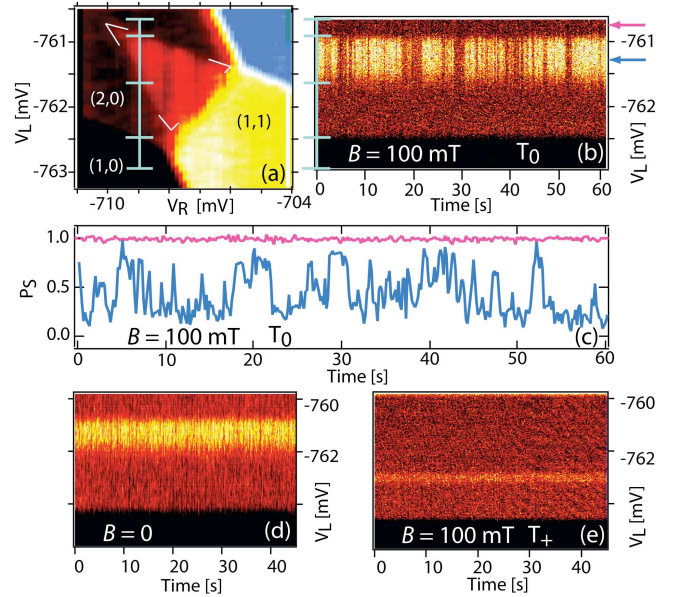


FIG. 2: (Color online) (a) rf-QPC sensor output V_{rf} as a function of V_L and V_R with gate-pulse cycle applied ($\tau_S = 25$ ns, $\tau_M = 1.6$ μ s, $B = 100$ mT). Color scale as in Fig. 1. (b) Repeated slices of V_L with $V_R = -709$ mV as a function of time. Markers on left axis correspond to markers in (a). (c) Sensor output calibrated to P_S (blue) along with a measurement of the background QPC noise (pink) from (b) at arrow positions. Bandwidth limited to ~ 3 Hz. (d) Similar to (b) but for $B = 0$, color scale same as in Fig. 1. (e) Similar to (b) but with S -point at S - T_+ degeneracy, $B = 100$ mT, color scale same as in Fig. 1.

$C = (1 - e^{-\tau_M/T_1})T_1/\tau_M$ [10] that relates P_S to the value P'_S corresponding to infinite T_1 , $1 - P_S = (1 - P'_S)C$. The dependence of P_S on τ_M (for a fixed $T_1 \sim 16$ μ s and $\tau_S = 50$ ns) is shown in Fig. 1(f). Applying this factor to Fig. 1(e) gives $P'_S(\tau_S \gg T_2^*) = 1/3$, consistent with theory [30], with no arbitrary scaling of sensor output.

With less temporal averaging, P_S shows fluctuations that reflect the dynamics of the Overhauser magnetic field. Figure 2 shows a slice through the readout triangle, obtained by rastering V_L at fixed V_R , with $B = 100$ mT, $\tau_S = 25$ ns. The extended slice allows fluctuations in P_S to be calibrated and compared to background noise. At $B = 100$ mT, fluctuations in P_S have a “blinking” appearance with broadband time dependence extending to several seconds. Fluctuations are ~ 100 times larger than the background charge noise. In contrast, at $B = 0$, slices across the readout triangle show no low-frequency structure in the P_S noise, with amplitude comparable to the background charge noise (Fig. 2(d)). Figure 2(e) shows slices across the $S - T_+$ resonance (see Fig. 1(d)). Here we avoid rapidly cycling through the $S - T_+$ transition, which can produce DNP [23]. Fluctuations in P_S associated with mixing S and T_+ show no low-frequency structure, independent of B and with a noise level comparable to background charge noise.

To investigate the spectral content of P_S fluctuations,

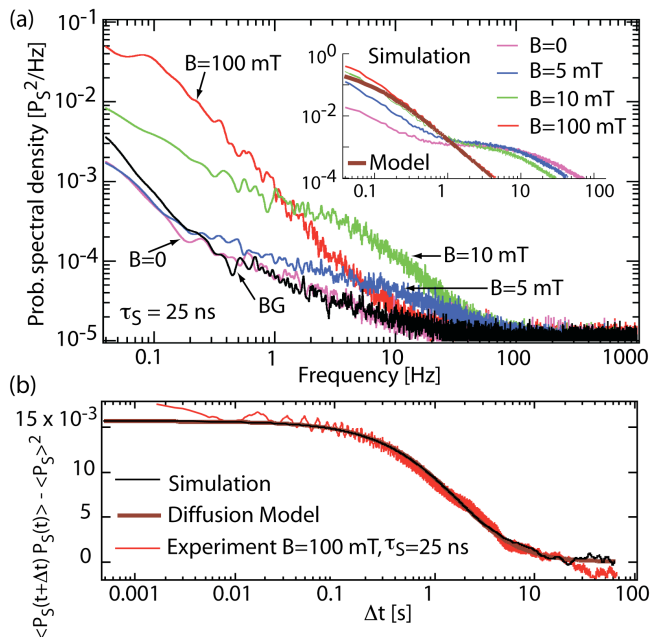


FIG. 3: (Color online) (a) Power spectra of P_S at various magnetic fields, $\tau_S = 25$ ns. Spectra obtained by FFT (with Hamming window) of average of 8 traces sampled at 10 kHz. Background measurement noise (BG) found by setting $\tau_S = 1$ ns at $B = 100$ mT. Inset: numerical simulation results for corresponding magnetic fields: $B = 0$ (pink), $B = 5$ mT (blue), $B = 10$ mT (green), $B = 100$ mT (red). (b) Autocorrelation P_S for $\tau_S = 25$ ns and $B = 100$ mT (red curve). Model function (Eq. 1) (brown) and Monte Carlo result (black).

fast Fourier transforms (FFTs) of V_{rf} are taken with V_L and V_R positioned to sample the center of the readout triangle. Figure 3(a) shows power spectra of P_S , with $\tau_S = 25$ ns, over the range $B = 0 - 100$ mT. Measurement at $\tau_S = 1$ ns, where $P_S \sim 1$, has a $1/f$ form and is identical to the noise measured outside the readout triangle, and constitutes our background of instrumental noise. At $B = 0$ no spectral content above the $1/f$ background noise is seen (Fig. 2(a)). With increasing B , an increasing spectral content is observed to be broadband below ~ 100 Hz. For $B > 20$ mT, the spectra become independent of B , and resemble the representative data shown for $B = 100$ mT.

The dependence of the power spectrum of P_S on separation time τ_S is shown in Fig. 4. We found that the largest fluctuations over the greatest frequency range occur for $\tau_S \sim T_2^* \sim 15$ ns, and these fluctuations show a roughly $1/f^2$ spectral dependence. Spectra were also obtained out to 100 kHz (not shown) where no additional high frequency components were observed above the background noise. For $\tau_S < T_2^*$, P_S remains near unity with few fluctuations; For $\tau_S > T_2^*$ low-frequency content is suppressed while components in the range 1 – 10 Hz are enhanced.

We model fluctuations in P_S as arising from the dynamic Overhauser magnetic field in thermal equilibrium. A classical Langevin equation is used to describe fluctu-

ations of $\Delta \mathbf{B}_{nuc}$ arising from nuclear spin diffusion on distances much larger than the lattice spacing and times much longer than the time-scale set by nuclear dipole-dipole interaction. For $B \gg B_{nuc}$, correlations of the Overhauser field can be evaluated analytically in terms of a dimensionless operator \hat{A}_z^β for each nuclear spin species β , where $\sum_\beta x^\beta \hat{A}_{z,l}^\beta \equiv \mathbf{B}_{nuc,z}^l / B_{nuc}$ and similarly for the right dot, with $x^{75\text{As}} = 1$, $x^{69\text{Ga}} = 0.6$, $x^{71\text{As}} = 0.4$. This gives $\langle \hat{A}_z^\beta(t + \Delta t) \hat{A}_z^\beta(t) \rangle = [(1 + \Delta t D_\beta / \sigma_z^2)(1 + \Delta t D_\beta / \sigma_\perp^2)]^{-1}$, at time difference Δt , where D_β is the species-dependent spin diffusion coefficient, σ_z is the electron wave function spatial extent perpendicular to the 2DEG (and along the external field) and σ_\perp is the wave function extent in the plane of the 2DEG, assumed symmetric in the plane. Brackets $\langle \dots \rangle$ denote averaging over t and nuclear ensembles.

Statistics of P_S are found using the z -component of the Overhauser operators, $\Delta \hat{A}_z = \sum_\beta x^\beta (\hat{A}_{z,l}^\beta - \hat{A}_{z,r}^\beta)$. For gaussian nuclear field fluctuations and a species-independent diffusion constant, D , this gives a mean value $\langle P_S \rangle = \frac{1}{2} [1 + e^{-2G^2 \langle \Delta \hat{A}_z^2 \rangle}]$ and autocorrelation $\langle P_S(t + \Delta t) P_S(t) \rangle - \langle P_S \rangle^2$

$$= \frac{e^{-4G^2 \langle \Delta \hat{A}_z^2 \rangle}}{4} \left[\cosh(4G^2 \langle \Delta \hat{A}_z(t + \Delta t) \Delta \hat{A}_z(t) \rangle) - 1 \right], \quad (1)$$

where $G = \tau_S / T_2^*$ is a gain coefficient. The autocorrelation function at $B = 100$ mT shown in Fig. 3(b) is obtained by inverse Fourier transforming the power spectrum [31]. We fit to the autocorrelation function using the contrast factor C , (see Fig. 1(f) and discussion), and the diffusion coefficient, D as fitting parameters. Wavefunction widths are taken from numerical simulations of the device [32], $\sigma_z = 7.5$ nm, $\sigma_\perp = 40$ nm. The fit gives $D \sim 10^{-13}$ cm²/s, consistent with previous measurements on bulk GaAs samples using optical techniques [6]. In Eq. (1) the dependence on τ_S leads to a scaling of the correlation time of P_S by G^2 to find the underlying Overhauser field correlation time. For fields $B > 20$ mT, the data in Fig. 3(b) indicate an autocorrelation time of ~ 3 s for P_S corresponding to a time $\tau_d \sim 10$ s for ΔA_z to decorrelate by half of its initial value.

Near $B \sim 0$, transverse components of the nuclear field lead to rapid dephasing of nuclear spins. In this regime, we use a Monte Carlo method to simulate nuclear dynamics [33]. Figure 3(b) shows that numerical and analytical approaches agree at higher fields, where both methods are applicable. Numerical power spectra for $B \sim 0$ are shown in the inset of Fig. 4.

We note some general features of the power spectra. First, the overall magnitude of the experimental data is reduced by contrast factor C compared to theory, as explained above. Also, $1/f$ background noise contributes spectral content below 10 Hz that is not present in the theory. Experiment and theory both show reduced low-frequency spectral content as B decreases toward zero. This can be understood as arising from the influence of the transverse nuclear fields at low B , which rapidly de-

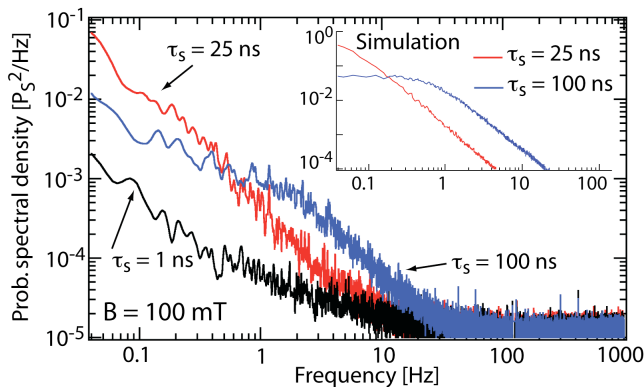


FIG. 4: (Color online) Power spectra of P_S at $B = 100$ mT for separation times $\tau_S = 25$ ns (red) and $\tau_S = 100$ ns (blue). Setting $\tau_S = 1$ ns (black) yields background noise. Inset shows simulation results for $B = 100$ mT, $\tau_S = 25$ ns (red) and $\tau_S = 100$ ns (blue). Note the suppression of low-frequency content and enhancement of mid-frequency content for long τ_S in the experiment and simulation.

phase nuclear spins and suppress long time correlations in ΔB_{nuc} . Similar behavior, though independent of B , is observed in the spectra of P_S at the $S-T_+$ resonance (not shown), since mixing between singlets and T_+ triplets is due to the transverse nuclear fields. Below $B \sim 10$ mT, an increased spectral content at mid-range frequencies, roughly between 1 - 10 Hz, is observed in the data and qualitatively captured by the simulations. The frequency at which the spectra intersect however, remains constant (~ 1 Hz) in the simulations but increases at low B in the experimental data. We are able to approximate this behavior in the simulation by increasing the diffusion coefficient ($D \sim 10^{-12}$ cm²/s at $B = 0$), implying an enhancement of diffusion, beyond typical values [6], as B approaches zero. This may be due to the growing influ-

ence of non-secular terms in the dipole-dipole interaction at low magnetic field [20, 27]. Diffusion maybe further enhanced at low B as a result of electron mediated flip-flop of nuclear spins [28, 34], an effect neglected in the simulation.

Finally, we model how the separation time for the two-electron spin state affects the power spectra. Simulated spectra are shown in the inset of Fig. 4 for $\tau_S = 1$ ns, 25 ns and 100 ns at $B = 100$ mT. Good agreement with experiment is achieved when again accounting for the additional $1/f$ noise and contrast reduction. We find that τ_S acts to filter fluctuations in ΔB_{nuc} , so that for $\tau_S \gg T_2^*$, low frequency correlations in ΔB_{nuc} are suppressed in the spectra of P_S (see Eq. 1). This filtering effect leads to the turn-over at ~ 2 Hz evident in the spectra for $\tau_S = 100$ ns. For $\tau_S \sim T_2^*$, little filtering occurs and the power spectra of P_S reflect the underlying intrinsic fluctuations of the Overhauser magnetic field.

In conclusion, by employing the high bandwidth and sensitivity of the rf-QPC, we have used the real-time mixing of singlet and triplet spin-states as a probe of hyperfine fluctuations in a GaAs double quantum dot. At fields above ~ 20 mT, fluctuations are well described by the statistics of nuclear spin diffusion, and decorrelate on a time, $\tau_d \sim 10$ seconds. We anticipate that the measurements presented here, showing the spectral dependence of these fluctuations and their evolution with magnetic field will be of use in the construction of protocols to extend coherence in these systems.

We thank L. DiCarlo, A. C. Johnson, and M. Stopa for contributions. This work was supported by DARPA, ARO/IARPA, NSF-NIRT (EIA-0210736) and Harvard Center for Nanoscale Systems. Research at UCSB supported in part by QuEST, an NSF Center.

-
- [1] D. Loss and D. DiVincenzo, Phys. Rev. A. **57**, 120 (1998).
 [2] B. E. Kane, Nature (London) **393**, 133 (1998).
 [3] S. I. Erlingsson, Y. V. Nazarov, and V. I. Fal'ko, Phys. Rev. B. **64**, 195306 (2001).
 [4] I. A. Merkulov, A. L. Efros, and M. Rosen, Phys. Rev. B. **65**, 205309 (2002).
 [5] A. V. Khaetskii, D. Loss, and L. Glazman, Phys. Rev. Lett. **88**, 186802 (2002).
 [6] D. Paget, G. Lampel, and B. Sapoval, Phys. Rev. B. **15**, 5780 (1977).
 [7] A. S. Bracker et al., Phys. Rev. Lett. **94**, 047402 (2005).
 [8] J. R. Petta et al., Science **309**, 2180 (2005).
 [9] F. H. L. Koppens et al., Nature (London) **442**, 766 (2006).
 [10] A. C. Johnson et al., Nature (London) **435**, 925 (2005).
 [11] F. H. L. Koppens et al., Science **309**, 1346 (2005).
 [12] A. K. Huttel et al., Phys. Rev. B. **69**, 073302 (2004).
 [13] J. M. Taylor et al., Nature Physics (London) **1**, 177 (2005).
 [14] G. Giedke et al., Phys. Rev. A. **74**, 032316 (2006).
 [15] D. Klauser, W. A. Coish, and D. Loss, Phys. Rev. B. **73**, 205302 (2006).
 [16] W. M. Witzel and S. Das Sarma, Phys. Rev. B. **74**, 035322 (2006).
 [17] S. A. Crooker et al., Nature (London) **431**, 49 (2004).
 [18] T. Sleator et al., Phys. Rev. Lett. **55**, 1742 (1985).
 [19] C. L. Degen et al., Phys. Rev. Lett. **99**, 250601 (2007).
 [20] A. Abragam, *Principles of Nuclear Magnetism (International Series of Monographs on Physics) Oxford University Press, USA* (1983).
 [21] D. Gammon et al., Science **277**, 85 (1997).
 [22] J. Baugh et al., Phys. Rev. Lett. **99**, 096804 (2007).
 [23] J. R. Petta et al., Phys. Rev. Lett. (in press) and arXiv:0709.0920 (2007).
 [24] K. Ono and S. Tarucha, Phys. Rev. Lett. **92**, 256803 (2004).
 [25] M. S. Rudner and L. S. Levitov, Phys. Rev. Lett. **99**, 036602 (2007).
 [26] O. N. Jouravlev and Y. Nazarov, Phys. Rev. Lett. **96**, 176804 (2006).
 [27] R. de Sousa and S. Das Sarma, Phys. Rev. B. **68**, 115322 (2003).

- [28] W. Yao, R.-B. Liu, and L. J. Sham, Phys. Rev. B. **74**, 195301 (2006).
- [29] D. J. Reilly et al., App. Phys. Lett. **91**, 162101 (2007).
- [30] J. M. Taylor et al., Phys. Rev. B. **76**, 035315 (2007).
- [31] The correlation function for the experimental data becomes slightly negative at long times, likely as the result of $1/f$ noise in the rf-QPC.
- [32] M. Stopa, Private communication, (2007).
- [33] J. M. Taylor, unpublished.
- [34] C. Deng and X. Hu, Phys. Rev. B. **73**, 241303(R) (2006).